Available online at www.sciencedirect.com

SCIENCE DIRECT®

Earth and Planetary Science Letters 225 (2004) 105–113

EPSL

www.elsevier.com/locate/epsl

Lower-mantle seismic discontinuities and the thermal morphology of subducted slabs

Christine Thomas[a,*], J-Michael Kendall[b,1], Julian Lowman[b,2]

[a] Department of Earth and Ocean Sciences, University of Liverpool, 4, Brownlow Street, Liverpool L69 3GP, UK
[b] Department of Earth Sciences, University of Leeds, Leeds LS2 9JT, UK

Received 1 March 2004; received in revised form 17 May 2004; accepted 28 May 2004
Available online 20 July 2004
Editor: S. King

Abstract

The nature of the lowermost few 100 km of the mantle holds insights into the scale of convection of the Earth's mantle. Here we investigate the fine structure of this region using seismic migration of shear waves reflecting from velocity discontinuities near the core–mantle boundary (CMB), recorded by a dense network of European seismic stations. Two main features are found. One structure exhibits large-scale topography and can be explained by a sharp increase in seismic velocity 206–316 km above the CMB. The second structure lies 55–85 km above the CMB and marks a sharp reduction in velocity. To explain the origin of these discontinuities, we appeal to numerical simulations of three-dimensional (3D) mantle convection, incorporating rigidly moving plates. The plates organize the convective flow to allow for the development of large convection cells and cool sheet-like downwellings at a convergent plate boundary. The results suggest that, in places, observed seismic complexity in D″ discontinuity structure may be due to the thermal gradients resulting from the accumulation of cool subducted plate material at the CMB.

Keywords: array seismology; migration; D″ region; seismic discontinuities; geodynamic modelling; mantle convection

1. Introduction

A long-standing debate in geophysics has revolved around the degree of mass exchange between the upper and lower mantle. Tomographic images show slab structures extending well into the lower mantle, and in some places to the core–mantle boundary (CMB; e.g., [1]), thereby supporting the whole-mantle convection paradigm. However, tomographic results have also formed the basis for arguments for a compositionally distinct layer at the base of the mantle that might explain the source for the primordial geochemical signature observed in oceanic island basalts [2]. Resolving the issue of mass exchange may consequently require an understanding of the properties of the D″ region, the lowermost 300 km of the mantle.

* Corresponding author. Tel.: +44-151-794-5143.
E-mail addresses: tine@earth.leeds.ac.uk (C. Thomas), kendall@earth.leeds.ac.uk (J.-M. Kendall), j.lowman@earth.leeds.ac.uk (J. Lowman).
[1] Tel.: +44-113-343-5258.
[2] Tel.: +44-113-343-5212.

0012-821X/$ - see front matter © 2004 Elsevier B.V. All rights reserved.
doi:10.1016/j.epsl.2004.05.038

The anomalous nature of D″ has been recognised for nearly 70 years [3–5]. However, in recent years, seismic studies have illuminated the complexity of this region on a range of length scales through, for example, observations of small-scale structures or scatterers [6], ultralow velocity zones (ULVZs) [7] and seismic anisotropy close to the core–mantle boundary (CMB) [8,9]. It is the site of the largest lateral variations in velocities in the lower mantle [1,10]. There is also abundant evidence for a seismic discontinuity at the top of the D″ region [11,12] and data from seismic arrays have enhanced our images of this discontinuity [13,14]. The complexity of the region has often been used as an argument for chemical heterogeneity at the base of the mantle. Recently, seismic migration, a technique borrowed from oil exploration seismology, has been employed to determine the location of scatterers and the depth of such discontinuities [15–17]. This method tries to find the origin of scattered or reflected waves by back-projecting seismic energy to the likely place of scattering or reflection.

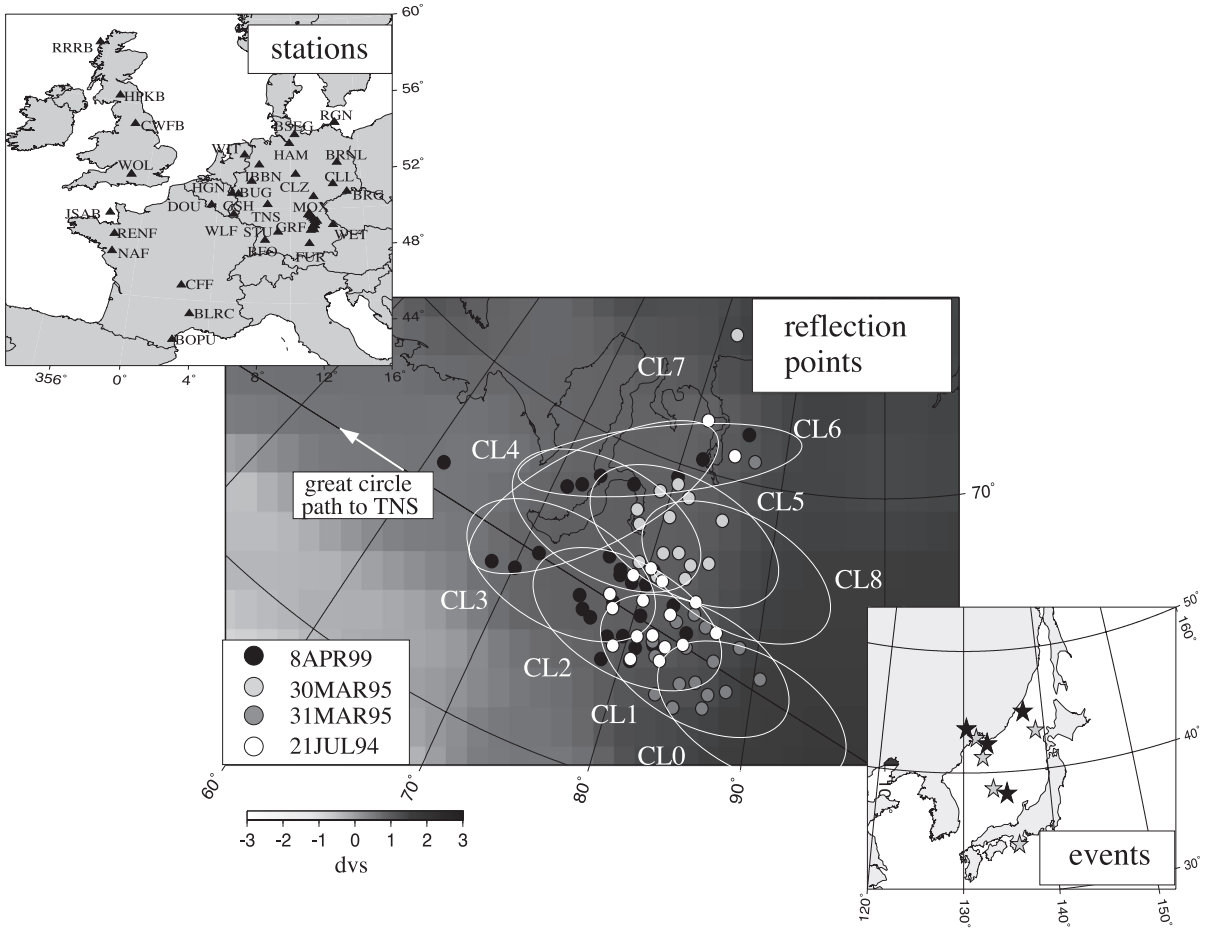

Fig. 1. Sources, receivers and reflection points in the lowermost mantle. The stations include permanent stations of the German Regional Network, stations in the Benelux countries as well as a temporary network across Britain and France (SPICED) [39]. The black stars mark events used in this study, grey stars are events that could not be used due to poor quality signals. The reflection points in the deep mantle (middle figure) are shown for the four events in different grey-scale circles. The ellipses indicate the clusters used in the migration and denote the approximate size of a Fresnel Zone for the seismic waves used in this study. The arrow points to the direction of the station TNS in Germany. The tomographic image is from [1], the grey-scale indicates the S velocity contrast in the lowest layer of the mantle.

2. Data analysis

Here, we have used a migration method [16] to study variations in D″ structure beneath northern Asia, looking for reflections from this region. Dense arrays of seismic stations in Europe are used to investigate events beneath the region of the eastern China–Russia border and Japan, yielding source–receiver distance ranges of 68°–82°. Such data illuminate reflection points in the deep mantle beneath northwestern Russia in an area approximately 10° by 20° (Fig. 1). This is a region where tomographic S wave models (e.g., [1]) indicate the end of a fast-velocity region, sometimes associated with the ancient Izanagi plate [18]. We look for energy in the coda of S waves that turn just above the D″ region. Should there exist a D″ discontinuity associated with a sharp increase in velocity, there will be a reflection from the top of the D″ region, here simply termed SdS. This wave consists of a reflection from the top of the D″ reflector and a diving wave that turns in the D″ region. These waves form a triplication in travel time [11]. Given the band-limited nature of seismic data, it is usually difficult to distinguish between the reflected and diving waves and we therefore simply refer to the signal as SdS. It is also possible that such a triplication will be produced by steep velocity gradients in the D″ region and not a discontinuity [19]. In order to map detailed variations in the topography of D″ discontinuities, we look for this signal using clusters of bounce points roughly the size of a Fresnel zone (220 by 440 km for SdS, with a dominant frequency of 6 s). We have performed the migration for all events and receivers in nine individual and slightly overlapping clusters. The grid spacing is 1° (~ 50 km) laterally and 10° vertically and the grid extends 28° by 35° (1680 by 1500 km) laterally and has 52 depth layers from the core–mantle boundary to 2200 km. Four earthquakes have been studied (Table 1): the number limited by the magnitude of the event, complexities in source functions and low signal to noise ratios.

Table 1
Events used in this study

Event	Date	Time	Latitude	Longitude	Depth
1	20 January 1994	13:37:02.1	27.89	139.40	498 km
2	30 March 1995	22:15:52.1	44.84	137.54	319 km
3	31 March 1995	14:01:40.1	38.21	135.01	354 km
4	8 April 1999	13:10:34.1	43.61	130.35	565 km

Earthquake parameters are from the Preliminary Determination of Earthquakes (PDE) Catalogue.

3. Migration results

An example of the results of migration for data within a single bounce-point cluster is shown in Fig. 2a. The technique starts by calculating travel times between a 3D grid of hypothetical reflection points and individual stations within a cluster. Seismic data from the cluster are then time-shifted by the predicted times and are summed for each hypothetical reflection point. The data will sum coherently should a grid point actually correspond to a point of reflected seismic energy. The left-hand side of Fig. 2a shows the results for four different depth slices. The bottom slice (depth of 2888 km) shows coherent positive amplitudes corresponding to S wave energy reflected from the CMB (i.e., the ScS phase). The second layer shows the focusing of negative amplitude energy at a depth of 2825 km. A ring of high amplitudes can be seen in this figure around the centre of the reflection area. These high amplitudes show ScS, the reflection from the CMB, which would arrive several seconds later than SdS at this depth. This is the expected behaviour for migration if the sources and receivers are far apart; the migrated image will focus to a point at the location of a true reflector. If the migration is applied to neighboring depth slices above this point, this image will defocus into circles following the isochrones around this point. The layer at a 2755 km depth shows no focusing of energy, indicating that there is no structure at this depth that produces a reflection. The top slice, 2645 km deep, shows clearly focussed positive amplitude energy.

The results of the migration show a positive amplitude reflection at depths that range between 2545 and 2705 km, depending on the cluster (Fig. 3). This reflection has the same polarity as the lower-mantle turning S wave and the ScS wave and suggests an increase in impedance. We interpret the signal as a reflection from a seismic discontinuity at the top of D″. Other studies have shown evidence for both P and S wave discontinuities in this region and, taken together, they suggest considerable variability in the

distance of the reflector from the CMB. An average reflector depth of 2605 [15,20] and 2650 km [17], respectively, for both P and S waves has been observed for this region, but other studies have shown large variations in the depth of the discontinuity [21]. Previous studies have normally used estimates based on inversions for one-dimensional (1D) structure. However, Freybourger et al. [17] also used a migration technique but used a set of European stations to estimate a single reflection point. Our results suggest more dramatic variations in topography (186 to 345 km from the CMB), most likely because we are using a more accurate migration method and clusters of bounce points.

Perhaps a more surprising result is the presence of a weaker reflector 55 to 85 km above the CMB. The

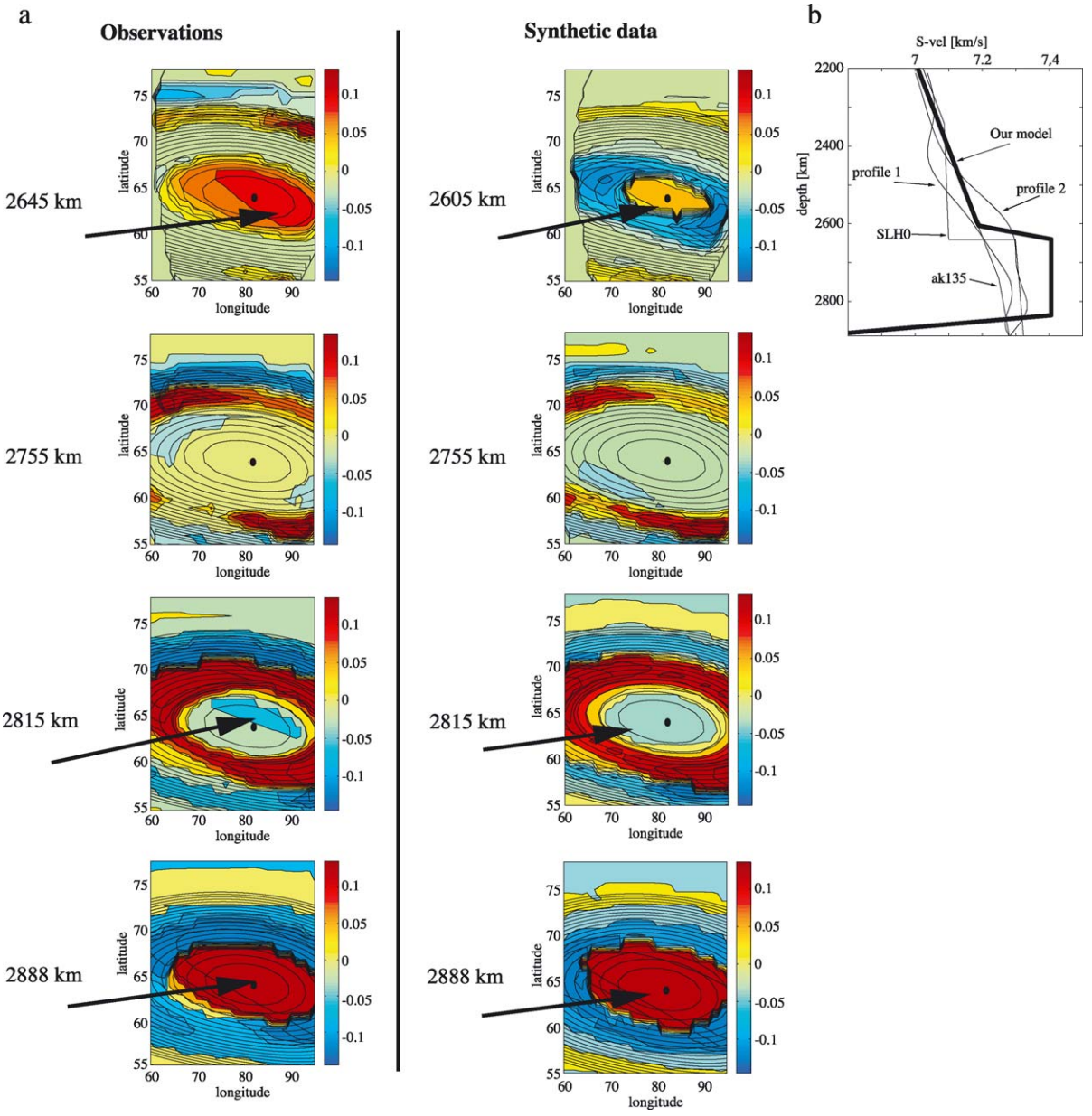

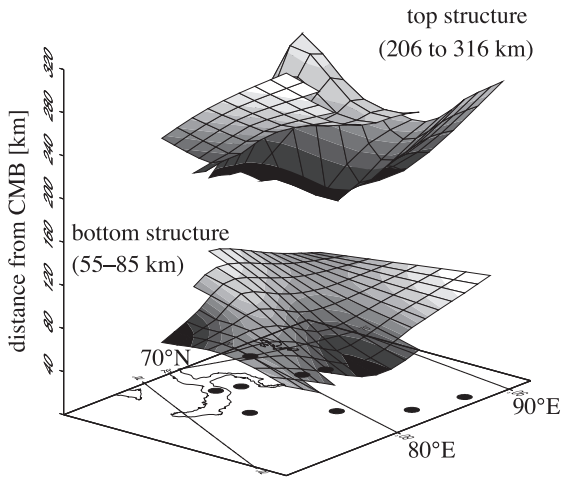

Fig. 3. The calculated topography of the two observed discontinuities. Results are a compilation from all clusters of bounce points and are shown on a mesh grid with interpolations between points. True reflection points from the middle of each cluster. The top structure shows strong topography from 206 to 316 km above the CMB with a positive impedance contrast, whereas the bottom structure exhibits much less topography (55–85 km above the CMB) and a negative impedance contrast. Dark grey regions mark lows and light grey regions show high points in the topography.

sign of the amplitude suggests a negative change in impedance and therefore a negative density and/or velocity jump. The topography of this second structure is much less than that observed at the top of the D″ region (Fig. 3). Because there is a decrease in impedance, reflections from this boundary are expected to be smaller that those from the upper boundary. Reflections from the positive upper boundary are larger due to near-critical angles of incidence.

4. Geodynamical constraints

To interpret our reflections, we appeal to a geodynamical mantle convection model that incorporates thick stiff plates in a 3D Cartesian geometry [22]. We use a hybrid spectral–finite-difference approach to model convection in a $3 \times 2 \times 1$ Cartesian geometry using a grid resolution of $486 \times 324 \times 162$. The velocities are solved using a propagator technique and the energy equation is solved using a flux-corrected finite-difference formulation [23]. We specify periodic (wrap around) boundary conditions on the vertical sidewalls of the calculations. The convection calculation features a depth-dependent viscosity based on a fit of postglacial rebound and free-air gravity anomaly data by Forte and Mitrovica [24], resulting in a viscosity profile that increases smoothly by a factor of 36 from the upper to the lower mantle. Recent work by Forte and Mitrovica [25] suggests that the viscosity of the lower mantle may vary sharply by orders of magnitude at several different depths with several reversals in gradient, but that the ratio of the mean lower mantle viscosity to the mean upper mantle viscosity is still approximately 40. Guided by the persistence in the relevant literature of a mean lower mantle to upper mantle viscosity of between 30 and 40 (e.g., [26–29]), we employ the smooth variation in mantle viscosity employed by Pysklywec and Mitrovica [30] as a first-order approximation of the increase in viscosity with depth through the lower mantle. However, we note that significant rapid increases (and decreases) in mantle viscosity structure could significantly affect our results. The upper 100 km of

Fig. 2. (a) Migration results for four different layers showing the focusing of amplitudes in the area around the geometric reflection point (black circle) for an S wave. The observations are displayed on the left side; the right-hand side shows the synthetic modelling results. For the observations (left-hand side), the layers are the core–mantle boundary (bottom layer), a layer at 2815 km depth (74 km above the core–mantle boundary), a layer at 2755 km depth in the middle of the D″ region and a layer at 2645 km depth, which in this case is the top of the D″ region. At the bottom layer, an amplification of amplitudes can be seen around the geometric reflection point. The amplitude is positive and denotes the ScS reflection. At 2815 km depth, a small area with a negative but amplified amplitude can be seen. The outer ring of high-positive amplitudes shows the S wave that arrives several seconds after the reflection from the layer at 2815 km depth. This moving outward of energy is typical for migration studies for which the sources and receivers are far apart (see text). At 2755 km depth, no focussed amplitude is visible in the area around the geometrical reflection point, showing that no structure is found in this depth. At 2645 km depth, a focusing of positive amplitude can be observed. On the right-hand side, the synthetic data show a very similar picture, but the depths of the layers vary slightly with those for the observations. (b) The model used to calculate synthetic data is shown as bold black line. The model has a gradient of +3% velocity change at the top of the D″ region and a −10% S velocity gradient in the lowest few tens of km. For comparison, the models ak135 [40] and SLHE [11] are given. SLHE has a discontinuity at the top of the D″ region, beneath which the high velocity continues down to the core–mantle boundary. Profiles 1 and 2 are velocity profiles derived for the locations where the temperature field of the geodynamic modelling (Fig. 4) is sampled.

our model, the stiff plates, is 1000 times more viscous than the upper mantle immediately below. Similarly, the static plate geometry is specified a priori. However, the time-dependent plate velocities evolve dynamically in accordance with a force-balance method [31]. Consequently, plate motion is determined by the buoyancy distribution within both the plates and the underlying mantle, and the temperature of subducted plate material reflects the history of the plate velocity that is consistent with the other model parameters. Heating is supplied by a combination of an isothermal bottom boundary and uniformly distributed, temporally invariant internal heat sources. The resulting ratio of basal heating to internal heating, as determined by the time-averaged surface heat flow, is approximately 1:1. The Benard–Rayleigh number of the calculation, based on the lower mantle viscosity, is 2.8×10 e6.

Fig. 4a shows two isosurfaces in a temperature field snapshot from a calculation that features two plates. Without the presence of the model plates, an internally heated convecting system in the parameter range we consider is characterized by short wavelength flow in the upper thermal boundary layer of the system (e.g., [32]). The plate size affects the convective wavelength of the system (e.g., [41,42]), and therefore, the temperature of subducted plate material relative to the temperature of fluid below. The convergence of the model plates along the specified linear plate boundary results in the formation of a downwelling sheet of cold material that begins to descend through the mantle, with a morphology and temperature that reflects the linearity of the plate boundary and the size of the plate, respectively. The sheet-like downwelling descends with little deformation until it reaches the lower boundary of the system. In contrast, upwelling material breaks away from the lower thermal boundary layer in sheets but rapidly organizes into cylindrical plume-like features while traversing the deep mantle. Cool material spreads laterally across the base of the system (modelled CMB) upon arrival. There is considerable structure on the upper boundary of this cold isosurface. Moreover, due to variations in plate velocity (and hence subduction rates) sections of cold slab detach from the supply of the downwelling flow, resulting in distinct sheets of cold material accumulating in some regions at the base of the convecting system while other regions may be void of the remnants of cool ancient plates.

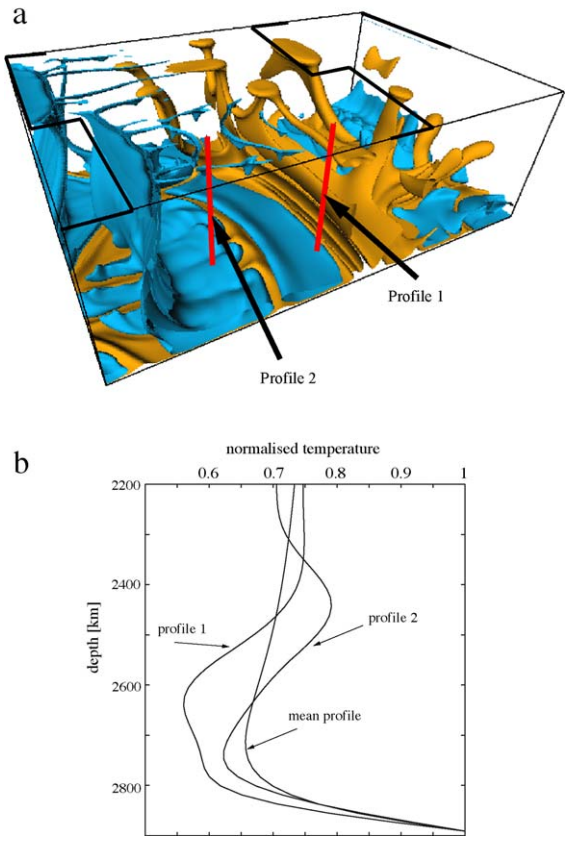

Fig. 4. (a) Temperature field snapshot from a mantle convection calculation showing slab-like downwellings accumulating in the lowermost mantle. Thick black lines at the surface of the box indicate plate boundaries. The slabs, after sinking down to the base of the model, move out horizontally and exhibit strong undulations in their upper surfaces. The base of the slabs shows very little topography. Red vertical lines indicate locations where the temperature field is sampled. (b) The temperature models calculated at the locations shown in panel a. The mean profile is the average temperature profile in the convection model. The profiles that go through a slab (cold) region show large positive gradients at a depth of 2300 km and below. Much steeper negative-gradients lie on the underside of the slab structure. For the interpretation of the references to colour in this figure legend, the reader is referred to the web version of this article.

An example of the lateral variations in thermal structure of the lowermost mantle is also illustrated in Fig. 4b by showing vertical temperature profiles, for fixed horizontal co-ordinates, through the temperature

field snapshot presented in Fig. 4a. In regions containing the remnants of slab material, there are relatively sharp decreases in temperature a few hundreds of kilometers above the modelled CMB and very sharp increases in temperature much nearer the CMB. Profiles through ambient parts of the temperature field show a simple increase in temperature near the CMB.

We constructed a velocity profile loosely based on thermal profiles for the downwelling regions (Fig. 2b, thick black line) and used the reflectivity method [33] to model wave propagation through the resulting structure.

A rigorous temperature to velocity conversion is unwarranted, given the implicit approximations made in the mantle convection calculations. Some of the most important simplifications specified include the use of a Cartesian geometry, the allowance of two-sided subduction at convergent boundaries, the neglect of a depth-dependent thermal expansion coefficient and the negligence of temperature-dependent viscosity (implying that the slabs in our calculations are strictly thermal features). Moreover, the scaling constants are not well known for the lowermost mantle. Nevertheless, because our calculations incorporate the full thermal history of a dynamically consistent, large, thick plate cooling in a whole-mantle calculation, the thermal signature of the subducted material in our model is more realistic than in previously applied calculations [34].

A sharp increase in velocity gradient at the top of D″ will produce a travel time triplication and, hence, ScS precursors. With real data, it can be difficult to distinguish between such a velocity gradient and a discontinuity [19]. A sharp negative gradient will also backscatter low-frequency seismic energy, again producing an apparent seismic reflection. The synthetic waveforms for this model are migrated in the same way as the data, and Fig. 2 shows that there is good agreement between the data and the synthetics for our model.

5. Discussion

The thermal models show large variations in the complexity of the upper boundary of the slab anomaly. The lower boundary, which represents the hot CMB boundary condition, is at a more uniform height. These features are also born out in our observations. The negative-amplitude lower-boundary reflections have not been noticed before, probably due to their weakness—they are not normally visible in the raw seismograms—but Gaherty and Lay [35] reported the observation of a second positive reflection in this region, indicating layering within the D″ region. It is interesting to speculate whether or not the lower boundary could generate signals associated with ultralow velocity zones (ULVZs) [7]. However, our reflector is much further from the CMB than the proposed top boundary of ULVZs.

Our results suggest that much of the complexity in discontinuity structure in the lowermost mantle beneath northern Asia can be explained by the thermal structure of a slab that has been subducted to the base of the mantle. This does not preclude the possibility of compositional anomalies in D″. It has been suggested that downwelling slab material may bulldoze away primordial material accumulated at the CMB [21]. Comparative variations in shear velocities and bulk-sound-speed agree in slab regions, supporting thermal anomalies but disagreeing low-velocity regions, supporting chemical anomalies [10]. There is also the question of the fate of oceanic crust in the lowermost mantle. Its form and seismic properties at these pressures and temperatures are poorly understood at this time. Inclusions of such material may explain lower-mantle scatterers [16,36] or even seismic anisotropy [8]. However, it can be difficult to explain the seismic properties of D″ with a simple chemical layer alone [37].

6. Conclusions

We have migrated ScS precursors to a 3D grid in the lowermost mantle beneath Eurasia detecting two discontinuities. The top reflector at approximately 300 km above the CMB shows an increase in S wave speed and large topography, whereas the second reflector at approximately 70 km above the CMB shows a negative velocity gradient with much less topography. The observed data can be explained using the temperature field of descending thermally defined slabs in simple geodynamic models that simulate the convergence of stiff plates in a 3D mantle convection

calculation, with a heating mode and depth-dependent viscosity in the parameter range appropriate for the Earth. We note that a strong increase in the viscosity stratification or the thermal expansion coefficient of the mantle could affect the descent of the cold material in a convecting system such as that which we modelled. Similarly, we do not model the influence of phase change boundaries on the descending material. Indeed, we consider investigating the influence of each of these complexities on the depth to which plates descend beyond the scope of this work. Rather, we aim to determine whether a thermal anomaly with a plate-like signature could explain our seismic observations in the case that the plate material does reach the CMB.

Our results are another piece of evidence that slabs may reach the CMB and that convection can operate on a whole-mantle scale. Our geodynamical simulations show that as slab-like thermal anomalies reach the CMB, they can emplace thermal features that can explain the origin of the seismic properties of the lowermost mantle in the regions sampled by our observations.

Acknowledgements

We would like to thank Mike Wysession and an anonymous reviewer for their helpful comments on the manuscript. Maps were produced using GMT [38]. CT was partly supported by DFG grant TH763/1-1.

References

[1] S.P. Grand, R.D. Van der Hilst, S. Widiyantoro, Global seismic tomography: a snapshot of convection in the Earth, GSA Today 7 (1997) 1–7.

[2] L.H. Kellogg, B.H. Hager, R.D. van der Hilst, Compositional stratification in the deep mantle, Science 283 (1999) 1881–1884.

[3] B. Gutenberg, Über Erdbebenwellen VIIA, Kgl. Ges. D. Wiss. Nachr. Heft 2 (1914) 125–177.

[4] C.G. Dahm, New values for dilatational wave-velocities through the Earth, Trans. - Am. Geophys. Union, (1934) 80–83.

[5] K.E. Bullen, Compressibility–pressure hypothesis and the Earth's interior, Mon. Not. R. Astron. Soc., Geophys. Suppl. 5 (1949) 355–368.

[6] P.M. Shearer, M.A.H. Hedlin, P.S. Earle, PKP and PKKP precursor observations: implications for the small-scale structure of the deep mantle and core, in: M. Gurnis, M.E. Wysession, E. Knittle, B.A. Buffett (Eds.), The Core–Mantle Boundary Region, American Geophysical Union, Washington, DC, 1998, pp. 37–55.

[7] E.J. Garnero, J. Revenaugh, Q. Williams, T. Lay, L.H. Kellogg, Ultralow velocity zones at the core–mantle boundary, in: M. Gurnis, M.E. Wysession, E. Knittle, B.A. Buffett (Eds.), The Core–Mantle Boundary Region, American Geophysical Union, Washington, DC, 1998, pp. 319–334.

[8] J.-M. Kendall, P.G. Silver, Investigating causes of D″ anisotropy, in: M. Gurnis, M.E. Wysession, E. Knittle, B.A. Buffett (Eds.), The Core–Mantle Boundary Region, American Geophysical Union, Washington, DC, 1998, pp. 97–118.

[9] T. Lay, Q. Williams, E.J. Garnero, L. Kellogg, M.E. Wysession, Seismic wave anisotropy in the D″ region and its implications, in: M. Gurnis, M.E. Wysession, E. Knittle, B.A. Buffett (Eds.), The Core–Mantle Boundary Region, American Geophysical Union, Washington, DC, 1998, pp. 299–318.

[10] G. Masters, G. Laske, H. Bolton, A. Dziewonski, The relative behaviour of shear velocity, bulk sound speed, and compressional velocity in the mantle: implications for chemical and thermal structure, in: S. Karato, et al., (Ed.), Earth's Deep Interior, American Geophysical Union, Washington, DC, 2000, pp. 63–87.

[11] T. Lay, D.V. Helmberger, A lower mantle S-wave triplication and the shear velocity structure of D″, Geophys. J. R. Astron. Soc. 75 (1983) 799–837.

[12] M.E. Wysession, T. Lay, J. Revenaugh, Q. Williams, E.J. Garnero, R. Jeanloz, L.H. Kellogg, The D″ discontinuity and its implications, in: M. Gurnis, M.E. Wysession, E. Knittle, B.A. Buffett (Eds.), The Core–Mantle Boundary Region, American Geophysical Union, Washington, DC, 1998, pp. 273–297.

[13] M. Weber, J.P. Davis, C. Thomas, K. Krüger, F. Scherbaum, J. Schlittenhardt, M. Körnig, The structure of the lowermost mantle determined from using seismic arrays, in: E. Boschi, G. Ekström, A. Morelli (Eds.), Seismic Modelling of Earth Structure, Instituto Nazionale di Geofisica, Rome, 1996, pp. 399–442.

[14] F. Scherbaum, F. Krüger, M. Weber, Double beam imaging: mapping lower mantle heterogeneities using combinations of source and receiver arrays, J. Geophys. Res. 102 (1997) 507–522.

[15] S.L. Bilek, T. Lay, Lower mantle heterogeneity beneath Eurasia imaged by parametric migration of shear waves, Phys. Earth Planet. Inter. 108 (1998) 201–218.

[16] C. Thomas, M. Weber, Ch. Wicks, F. Scherbaum, Small scatterers in the lower mantle observed at German broadband arrays, J. Geophys. Res. 104 (1999) 15073–15088.

[17] M. Freybourger, S. Chevrot, F. Krüger, U. Achauer, A waveform migration for the investigation of P wave structure at the top of D″ beneath northern Siberia, J. Geophys. Res. 106 (2001) 4129–4140.

[18] C. Lithgow-Bertelloni, M.A. Richards, The dynamics of Ce-

nozoic and Mesozoic plate motions, Rev. Geophys. 36 (1998) 27–78.
[19] X.-F. Liu, J. Tromp, A.M. Dziewonski, Is there a first-order discontinuity in the lowermost mantle? Earth Planet. Sci. Lett. 160 (1998) 343–351.
[20] M. Weber, P- and S-wave reflections from anomalies in the lower mantle, Geophys. J. Int. 115 (1993) 183–210.
[21] M.E. Wysession, Imaging cold rocks at the base of the mantle: the sometimes fate of slabs? in: G.E. Bebout, D. Scholl, S. Kirby, J.P. Platt (Eds.), Subduction: Top to Bottom, American Geophysical Union, Washington, DC, 1996, pp. 369–384.
[22] J.P. Lowman, S.D. King, C.W. Gable, The role of the heating mode of the mantle in intermittent reorganization of the plate velocity field, Geophys. J. Int. 152 (2003) 455–467.
[23] B. Travis, P. Olson, G. Schubert, The transition from two-dimensional to three-dimensional planforms in infinite-Prandtl-number thermal convection, J. Fluid Mech. 216 (1990) 71–91.
[24] A.M. Forte, J.X. Mitrovica, New inferences of mantle viscosity from joint inversion of long-wavelength mantle convection and post-glacial rebound data, Geophys. Res. Lett. 23 (1996) 1147–1150.
[25] A.M. Forte, J.X. Mitrovica, Deep-mantle high-viscosity flow and thermochemical structure inferred from seismic and geodynamic data, Nature 410 (2001) 1049–1056.
[26] B. Hager, Subducted slabs and the geoid: constraints on mantle rheology and flow, J. Geophys. Res. 89 (1984) 6003–6015.
[27] M.A. Richards, B.H. Hager, Geoid anomalies in a dynamic Earth, J. Geophys. Res. 89 (1984) 5987–6002.
[28] Y. Ricard, C. Vigny, Mantle dynamics with induced plate tectonics, J. Geophys. Res. 94 (1989) 17543–17559.
[29] C. Thoraval, M.A. Richards, The geoid constraint in global geodynamics: viscosity structure, mantle heterogeneity models and boundary conditions, Geophys. J. Int. 131 (1997) 1–8.
[30] R.N. Pysklywec, J.X. Mitrovica, Mantle avalanches and the dynamic topography of continents, Earth Planet. Sci. Lett. 148 (1997) 447–455.
[31] C.W. Gable, R.J. O'Connell, B.J. Travis, Convection in 3 dimensions with surface plates—generation of toroidal flow, J. Geophys. Res. 96 (1991) 8391–8405.
[32] F. Dubuffet, M. Rabinowicz, M. Monnereau, Multiple scales in mantle convection, Earth Planet. Sci. Lett. 178 (2000) 351–366.
[33] G. Müller, The reflectivity method: a tutorial, J. Geophys. 58 (1985) 153–174.
[34] C. Mériaux, A. Agnon, J.R. Lister, The thermal signature of subducted lithospheric slabs at the core–mantle boundary, Earth Planet. Sci. Lett. 160 (1998) 551–562.
[35] J.B. Gaherty, T. Lay, Investigation of laterally heterogeneous shear velocity structure in D″ beneath Eurasia, J. Geophys. Res. 97 (1992) 417–435.
[36] M.A.H. Hedlin, P.M. Shearer, P.S. Earle, Waveform stacks of PKP precursors: evidence for small-scale heterogeneity throughout the mantle, Nature 387 (1997) 145–150.
[37] I. Sidorin, M. Gurnis, Geodynamically consistent seismic velocity predictions at the base of the mantle, in: M. Gurnis, M.E. Wysession, E. Knittle, B.A. Buffett (Eds.), The Core–Mantle Boundary Region, American Geophysical Union, Washington, DC, 1998, pp. 209–230.
[38] P. Wessel, W.H.F. Smith, Free software helps map and display data, EOS, Trans. - Am. Geophys. Union 72 (1991) 445–446.
[39] J.-M. Kendall, G. Helffrich, SPICED: imaging the deep Earth, Astron. Geophys. 42 (2001) 26–29.
[40] B.N.L. Kennett, E.R. Engdahl, R. Buhland, Constraints on seismic velocities in the Earth from travel-times, Geophys. J. Int. 122 (1995) 108–124.
[41] S.J. Zhong, M. Gurnis, Dynamic feedback between a continent-like raft and thermal convection. J. Geophys. Res. 98 (1993) 12219–12232.
[42] J.P. Lowman, S.D. King, C.W. Gable, The influence of tectonic plates on mantle convection patterns temperature and heat flow. Geophys. J. Int. 146 (2001) 619–636.